JOURNAL OF GEOPHYSICAL RESEARCH: SPACE PHYSICS, VOL. 118, 5099–5108, doi:10.1002/jgra.50495, 2013

Photoelectrons in the Enceladus plume

A. J. Coates,[1,2] A. Wellbrock,[1,2] G. H. Jones,[1,2] J. H. Waite,[3] P. Schippers,[4]
M. F. Thomsen,[5,6] C. S. Arridge,[1,2] and R. L. Tokar[5,6]

Received 10 May 2013; revised 16 July 2013; accepted 3 August 2013; published 27 August 2013.

[1] The plume of Enceladus is a remarkable plasma environment containing several charged particle species. These include cold magnetospheric electrons, negative and positive water clusters, charged nanograins, and "magnetospheric photoelectrons" produced from ionization of neutrals throughout the magnetosphere near Enceladus. Here we discuss observations of a population newly identified by the Cassini Plasma Spectrometer (CAPS) electron spectrometer instrument—photoelectrons produced in the plume ionosphere itself. These were found during the E19 encounter, in the energetic particle shadow where penetrating particles are absent. Throughout E19, CAPS was oriented away from the ram direction where the clusters and nanograins are observed during other encounters. Plume photoelectrons are also clearly observed during the E9 encounter and are also seen at all other Enceladus encounters where electron spectra are available. This new population, warmer than the ambient plasma population, is distinct from, but adds to, the magnetospheric photoelectrons. Here we discuss the observations and examine the implications, including the ionization source these electrons provide.

Citation: Coates, A. J., A. Wellbrock, G. H. Jones, J. H. Waite, P. Schippers, M. F. Thomsen, C. S. Arridge, and R. L. Tokar (2013), Photoelectrons in the Enceladus plume, *J. Geophys. Res. Space Physics, 118*, 5099–5108, doi:10.1002/jgra.50495.

1. Introduction

[2] Photoionization is a key process in the ionospheres of many solar system objects [e.g., *Schunk and Nagy*, 2009], including Earth [*Coates et al*., 1985, 2011, and references therein], Venus [*Brace et al*., 1982; *Coates et al*., 2008], Mars [*Frahm et al*., 2006], Titan [*Coates et al*., 2007], the main ring environment of Saturn [*Coates et al*., 2005], and the broad magnetospheric region near the orbit of Enceladus [*Schippers et al*., 2009; *Cravens et al*., 2011].

[3] The energy spectrum of photoelectrons arising from this process depends on the incoming solar radiation and on the composition of the neutrals. A characteristic, distinctive peak feature at ~20–30 eV is usually associated with the 30.4 nm line in the solar spectrum interacting with the nitrogen atmosphere of Titan and the carbon dioxide-rich atmospheres of Venus and Mars. At Titan, for example, the photoelectron energy is 24.09 eV [e.g., *Coates et al*., 2011], though the observed energy may be modified by the spacecraft potential which is usually negative in high-density ionospheric regions, decreasing the observed energy. This feature can be used as the signature of photoelectrons and has been used to trace the magnetic connection from the sunlit ionosphere to different locations including the tail at Titan, Venus, and Mars and into the magnetosphere at Earth [*Coates et al*., 2007, 2008, 2011; *Wellbrock et al*., 2012]. Photoelectrons may provide a mechanism for plasma escape at Titan [*Coates et al*., 2012].

[4] The inner regions of Saturn's magnetosphere are supplied with plasma produced by photoionization, charge exchange, and electron impact ionization of a cloud of neutral water molecules [*Shemansky et al*., 1993; *Esposito et al*., 2005; *Young et al*., 2005; *Perry et al*., 2010] which dominates the particle density in these regions between ~3 and 8 Saturn radii, R_S. Cassini has shown that these neutrals emanate from Enceladus itself. This followed the discovery of a dynamic atmosphere [*Dougherty et al*., 2006] and vast plumes of neutrals [*Waite et al*., 2006], plasma [*Tokar et al*., 2006; *Tokar et al*., 2009], water clusters [*Coates et al*., 2010a], and neutral and charged dust particles [*Spahn et al*., 2006; *Jones et al*., 2009] emanating from tiger stripe features on the surface [*Porco et al*., 2006]. The region near Enceladus itself provides an environment containing plasma from Saturn's magnetosphere as well as from Enceladus and its plumes.

[5] The plasma environment of Enceladus is determined by the approximately corotating magnetosphere of Saturn and its interaction with (a) momentum loading through charge exchange and negative grain charging and (b) the plasma produced from the plumes via ion pickup. The interaction drives field-aligned currents which can reach the Saturn auroral region and produce an auroral spot [*Pryor et al*., 2011]. In addition to the corotating plasma (~eV to tens

[1]Mullard Space Science Laboratory, University College London, Dorking, UK.
[2]The Centre for Planetary Sciences at UCL/Birkbeck, London, UK.
[3]Southwest Research Institute, San Antonio, Texas, USA.
[4]LESIA, Observatoire de Paris, Meudon, France.
[5]Planetary Science Institute, Tucson, Arizona, USA.
[6]Los Alamos National Laboratory, Los Alamos, New Mexico, USA.

Corresponding author: A. J. Coates, Mullard Space Science Laboratory, University College London, Holmbury St. Mary, Dorking RH5 6NT, UK. (a.coates@ucl.ac.uk)

2169-9380/14/10.1002/jgra.50495

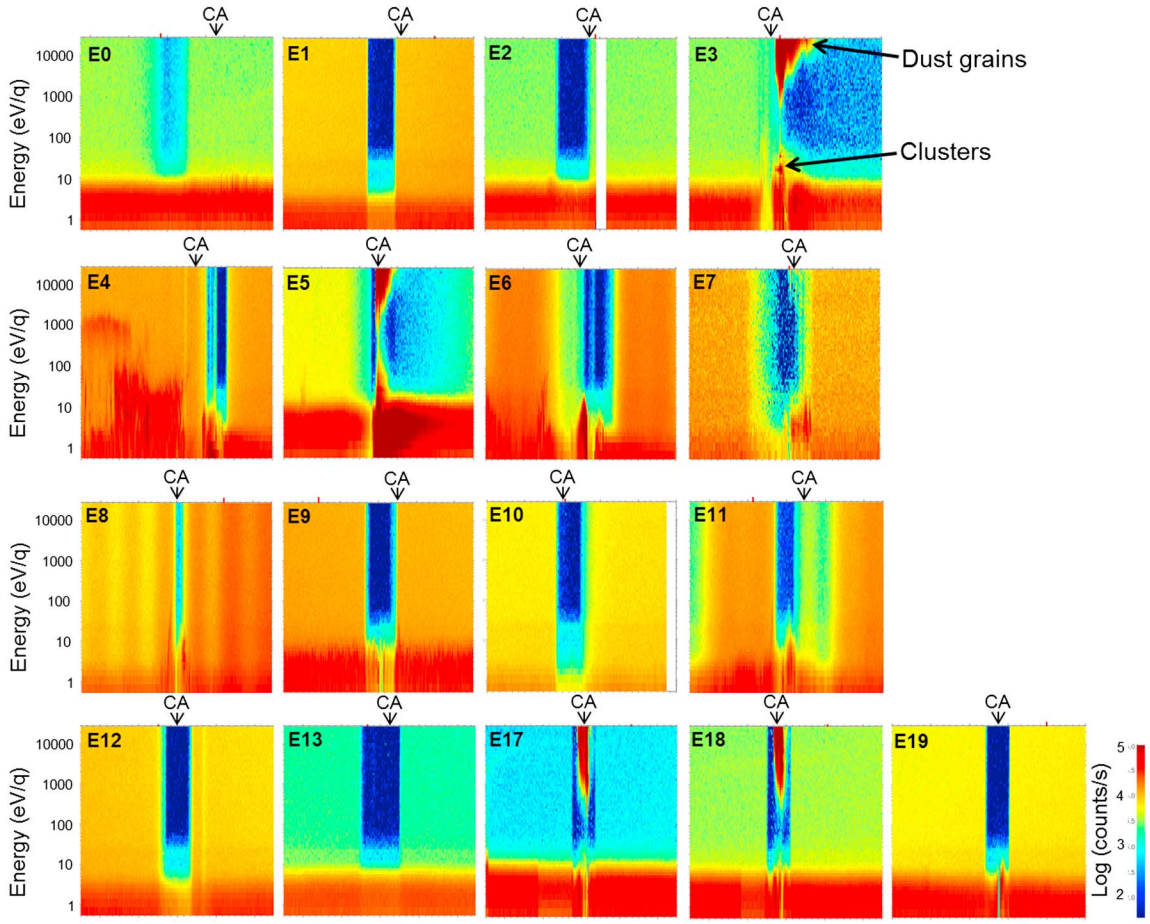

Figure 1. ELS spectrograms for all Enceladus encounters observed by CAPS. Ten minutes of data are shown in each case with closest approach (CA) indicated.

of eV), this region is populated by the trapped, higher-energy (~MeV) electrons in Saturn's radiation belts. An energy-dependent energetic particle "shadow" occurs as Enceladus itself absorbs the energetic particles. This is known as a "microsignature" and can be used to diagnose magnetosphere dynamics [e.g., *Jones et al*., 2006; *Roussos et al*., 2007]. It also provides the shielding used in this paper to distinguish the magnetospheric and photoelectron populations.

[6] During Enceladus encounters, an electron spectrometer (ELS) usually sees the magnetospheric electron population (up to about 20 eV; see also Figure 1) [e.g., *Coates et al*., 2010a]. The intensity of magnetospheric electrons diminishes very near Enceladus as electrons there are attached to ice grains [e.g., *Farrell et al*., 2009]. At a similar time, the ions are seen to slow significantly and, depending on the trajectory, may stagnate [*Tokar et al*., 2006; *Tokar et al*., 2009]. The observed magnetospheric electron signature at this location is not contaminated by spacecraft photoelectrons because the spacecraft potential is negative near Enceladus. During intervals of positive spacecraft potential, such spacecraft photoelectrons are trapped near the spacecraft and are seen at large fluxes at low energies. In addition, near the orbit of Enceladus, penetrating radiation contamination is typically observed across all energies (and anodes) in ELS, except when Cassini is in the energetic particle shadow of the moon.

[7] In the ram direction, ELS has detected two unexpected features in encountering the plasma plume of Enceladus. These are (1) water cluster ions [*Coates et al*., 2010a], seen as peaks corresponding to multiples of OH^-, up to ~500 eV/q, and (2) charged dust nanograins [*Jones et al*., 2009; *Hill et al*., 2012]. Away from the ram direction, and during the energetic particle shadow, magnetospheric and other electrons can be studied with very low background contamination, as the energetic particles are absorbed by Enceladus itself.

[8] In addition to the corotating plasma, Saturn's magnetosphere at the orbit of Enceladus contains photoelectrons produced from water and its products including oxygen [*Schippers et al*., 2009; *Cravens et al*., 2011]. This electron population, which we call "magnetospheric photoelectrons," appears throughout the inner magnetosphere of Saturn and again has a distinctive, peaked energy spectrum [*Schippers et al*., 2009]. The energy peak was observed at ~20 eV after correction of the modeled peak energy (~28 eV) for spacecraft potential. We note that photoelectrons of a similar peak energy and similar energy spectrum, but produced by local ionization in the plume, were modeled by *Ozak et al*. [2012].

[9] In this paper, we examine the region near Enceladus at several different encounters, in the region where the energetic particle shadow occurs. We observe the magnetospheric photoelectrons seen by *Schippers et al*. [2009] and,

Table 1. Summary of Enceladus Encounters (Enc) on the Date and Day of Year (DOY) Shown, With Closest Approach (CA) Given, Where There Are CAPS-ELS Data[a]

Enc	Date (DOY)	CA (h:min:s)	CA (km)	Ram ∠ During EPS (deg)	Ram	CA Upstream	Trajectory Orientation	Act	Plume	PA Near 0°, Notes
E0	17/2/05 (048)	03:30:29	1257	87 ± 20		U	Outbound			
E1	9/3/05 (068)	09:08:01	492	42–50 ± 10		U	Inbound			
E2	14/7/05 (195)	19:55:22	164	79–78 ± 10			S-N, inclined			
E3	12/3/08 (072)	19:06:12	47	9 + 10–7	Y		N-S, inclined		P	
E4	11/8/08 (224)	21:06:00	45	158–163 + 5–10			N-S, inclined		P	Pre-CA
E5	9/10/08 (283)	19:07:00	19	8–5 + 10	Y		N-S, inclined		P	
E6	31/10/08 (305)	17:15:00	191	60–150			N-S inclined	A	P	17:13
E7	2/11/09 (306)	07:42:00	91	10 ± 10	Y		Outbound		P	MCP bias low
E8	21/11/09 (325)	02:10:00	1594	22–25 ± 10			Inbound	A		02:09:30, 02:10:30
E9	28/4/10 (118)	00:11:00	91	64 ± 10			Outbound		P	
E10	18/5/10 (138)	06:04:00	192	10 ± 10	Y	U	Inbound			
E11	13/8/10 (225)	22:30:59	2542	80–40 ± 4			Inbound, S	A		22:29:10
E12	30/11/10 (334)	11:53:59	40	72 ± 10			Outbound, N pole			
E13	21/12/10 (355)	01:08:26	40	33 ± 10			Outbound, N pole			
E17	27/3/12 (087)	18:30:09	65	17–5 + 10	Y		Inbound		P	
E18	14/4/12 (105)	14:01:38	65	18–8 + 10	Y		Inbound		P	
E19	2/5/12 (123)	09:31:29	65	93 ± 10			Inbound		P	

[a]Ram and PA (Pitch Angle) refer to anode 5. EPS is the energetic particle shadow. Act column is marked A if CAPS is actuating. Plume column is marked "P" if the spacecraft traverses the 2 × 3 Enceladus radii (R_E) region below Enceladus' south pole. MCP refers to the ELS microchannel plate.

in addition, distinguish a new population of photoelectrons associated with ionization of plume material. This "plume photoelectron" population represents observations in the data of the photoelectrons seen in the *Ozak et al*. [2012] model. These photoelectrons, more energetic than the corotating plasma, together with the magnetospheric photoelectrons provide an additional source of ionization in this region of Saturn's magnetosphere.

2. Instrument and Flyby Orientation

[10] The data used here are from the Cassini Plasma Spectrometer (CAPS) [*Young et al*., 2004] electron spectrometer (ELS) [*Linder et al*., 1998]. ELS measures electrons in the energy range 0.6–28,800 eV/q, in each of eight 20° × 5° look directions, with an energy resolution of 16.7%, swept through its range once every 2 s. The instantaneous field of view is thus a 160° × 5° fan; this can be rotated by the CAPS actuator to increase the field of view. In most of the encounters studied here, the actuator is fixed to allow high time resolution in the selected direction. We analyze data from a single central anode with unobstructed field of view.

[11] The Enceladus encounters of Cassini are named "En" where n is the nth encounter during the mission. CAPS observations were available for 17 of these (these encounters are summarized in Table 1). The E19 encounter on 2 May 2012 executed a transverse trajectory through the Enceladus

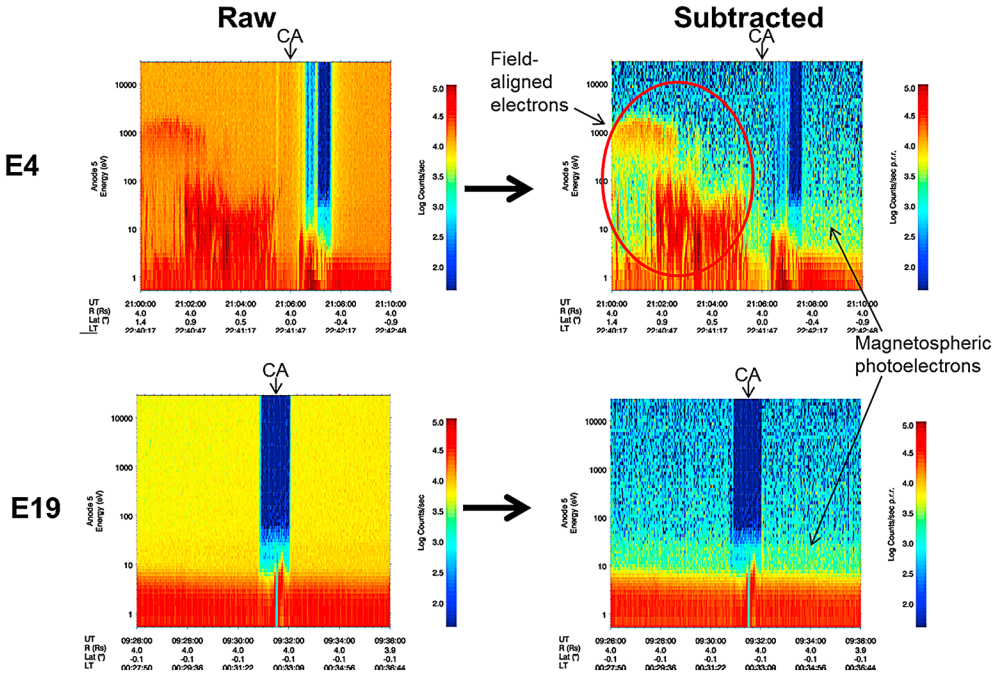

Figure 2. Penetrating radiation removal for E4 and E19.

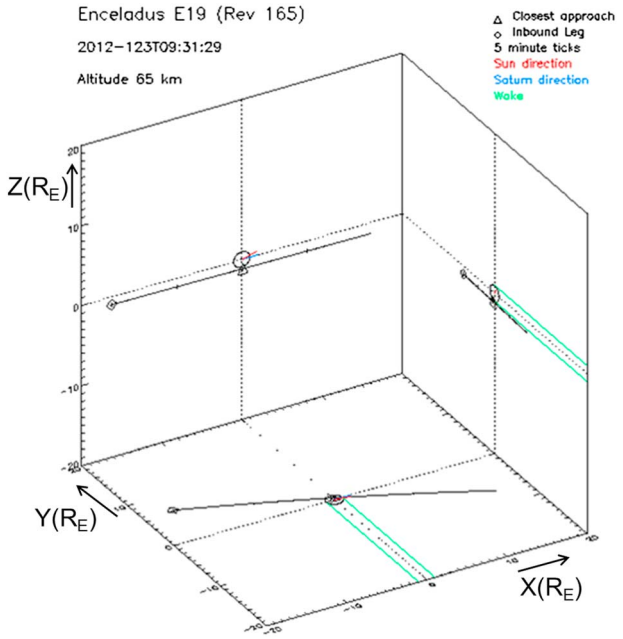

Figure 3. E19 encounter geometry. The *X* axis is from Enceladus to Saturn, *Y* is in the direction of orbital motion, and *Z* forms the right-handed set, directed northward.

plume with a closest approach of 65 km. The CAPS field of view was oriented well away from the spacecraft ram direction, allowing populations other than cluster ions [*Coates et al.*, 2010a] or charged nanograins [*Jones et al.*, 2009; *Hill et al.*, 2012] to be distinguished.

3. Observations

[12] In Figure 1, we show spectrograms from all of the Enceladus encounters where CAPS measurements are available. The format of each plot is count rate (color scale, proportional to differential energy flux, DEF) plotted as a function of energy (vertical axis) and time (horizontal, covering 10 min around closest approach). During all of the encounters, the overall structure shows a relatively high count rate across all energies (penetrating radiation) at the start and end of each plot, with a much lower count rate toward the center (the energetic particle shadow). The ELS is shielded by 1.6 mm of aluminum on average, so the penetrating radiation corresponds mainly to counts induced by electrons with energy >800 keV [see *Rymer et al.*, 2001]. The penetrating radiation count rate can therefore be used as a proxy for energetic electron flux in Saturn's radiation belts. A notable feature of the penetrating radiation is that it varies significantly between encounters, indicating the highly variable (factor >10) nature of Saturn's radiation belt electron fluxes [cf. *Kollmann et al.*, 2011].

[13] The penetrating radiation count rate is independent of the electrostatic analyzer settings and hence shows up as a count rate independent of energy; additional features are seen above this constant (within a sweep) count rate level in all the plots. At energies <20 eV, the count rate enhancement is due to magnetospheric electrons. These are cold, and the upper electron energy approximately follows the corotation velocity for protons in this region [*Young et al.*, 2005] due to collisional coupling with ambient ions [*Rymer et al.*, 2007]. There are variations in the magnetospheric electron population within many of the plots and between plots as conditions vary; within the region near Enceladus, this population can be significantly reduced. The plasma wake behind Enceladus is on the "downstream" side (relative to corotation), whereas the energetic electron wake is on the upstream side [e.g., *Roussos et al.*, 2007]. The well-defined energetic particle shadows seen in Figure 1 are from upstream passes. In downstream passes, the plasma wake is seen in some cases, though sharp

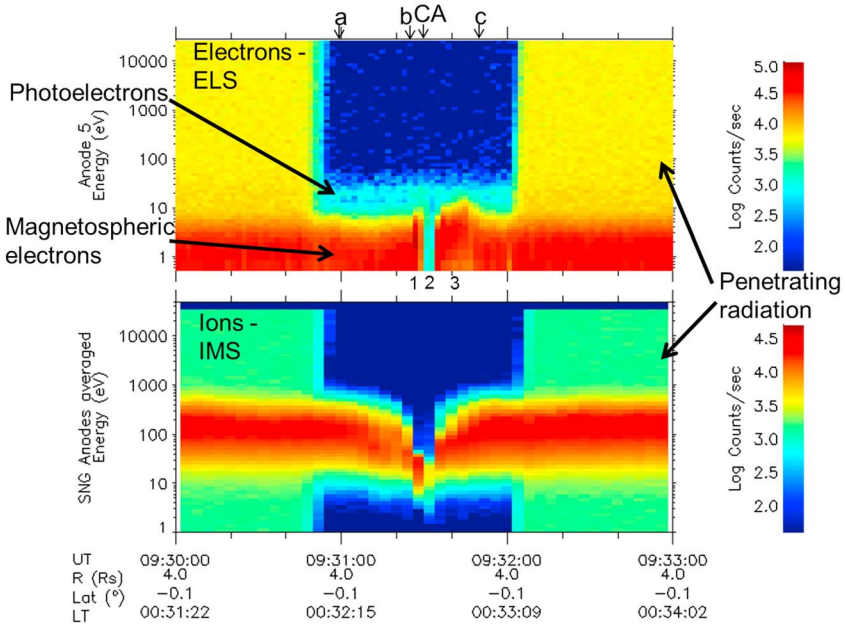

Figure 4. ELS and CAPS IMS singles (SNG) data from E19 encounter. Features 1, 2, and 3 and times of spectra a, b, and c are indicated (see text and Figure 5).

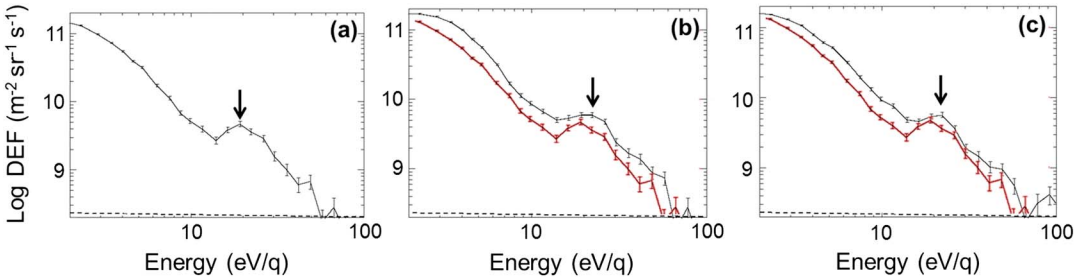

Figure 5. Electron spectra from the E19 encounter, averaged over five sweeps (10 s) from the marked start times: (a) 09:31:00, (b) 09:31:24, and (c) 09:31:50. The spectrum in Figure 5a is reproduced in red in Figures 5b and 5c for comparison.

reductions in the low-energy electrons are probably associated with charging of the dust.

[14] As shown in Table 1, the encounters are for a variety of viewing orientations. Encounters 3, 5, 7, 17, and 18 are ram pointed and through the plume (see Table 1). During these encounters, in Figure 1, we clearly observe the charged dust signatures at high energies (as discussed by *Jones et al*. [2009] for E3 and *Hill et al*. [2012] for E3, E5, and E7) as well as negative cluster ion signatures for E3 and E5 [*Coates et al*., 2010a]. Encounter E4 is arranged for ELS to view field-aligned electrons (0° pitch angles, denoted by "PA 0°" in Table 1). These electrons were associated with the Enceladus auroral spot in this encounter [*Pryor et al*., 2011]. Field-aligned intervals are also present during other encounters (see Table 1 and Figure 1). During all encounters in Figure 1, an interval of low penetrating radiation level is observed, with different durations depending on the flyby speed and encounter geometry. This is the energetic particle shadow, caused by the interception of radiation belt particles by Enceladus itself, and it is these intervals which allow additional populations to be distinguished.

[15] Outside the energetic particle shadow, reduction of the penetrating particle population can be achieved by subtracting a fixed count rate from all energies. To do this, we calculate the mean of the count rate in the top few energy channels for each sweep and subtract the resulting count rate from the observations at all energies. While better techniques are under development, this crude technique reveals some of the other populations in more detail. This is illustrated in Figure 2, for encounters E4 and E19. The field-aligned electron population is better seen in the subtracted plot, and the E19 plot, while still noisy due to statistical fluctuations, reveals a population at 20–30 eV across the plot. These are photoelectrons created in the magnetosphere near Enceladus as discussed by *Schippers et al*. [2009] and *Cravens et al*. [2011], but away from the moon, these are not directly dependent on the presence of Enceladus itself.

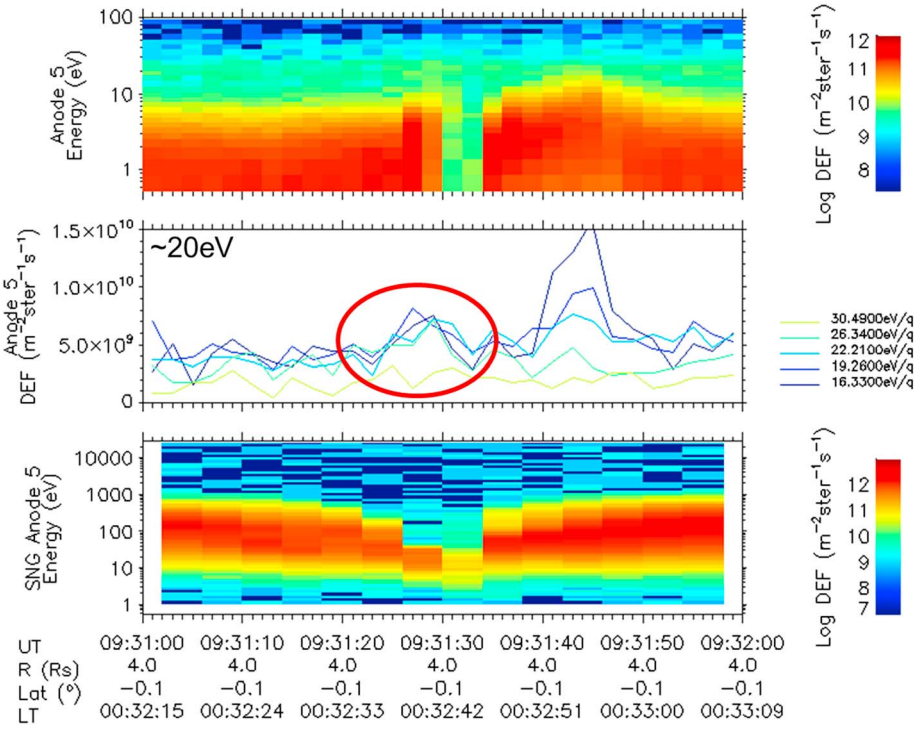

Figure 6. E19 data. (top panel) ELS spectrogram. (middle panel) ELS counts at indicated energies. (bottom panel) IMS spectrogram.

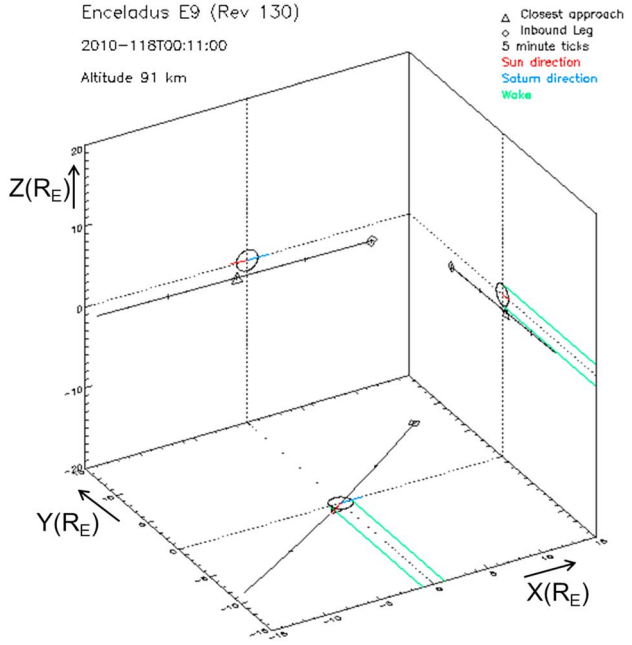

Figure 7. E9 encounter geometry. Axes as for Figure 3.

[16] The geometry of the E19 flyby is shown in Figure 3 as a low-altitude pass through the plume. The different feature of this encounter is that the ELS field of view in anode 5 is at ~90° to the ram direction, so that the measurements do not contain the ram direction features such as charged dust, negative ions, and plume ions. This allows us to analyze nonram electron populations in detail during this flyby.

[17] The ELS (top panel) and ion mass spectrometer (IMS; bottom panel) data from E19 are shown in Figure 4, for 3 min surrounding closest approach. The penetrating radiation is seen before ~09:30:50 and after ~09:32. The boundary of the energetic particle shadow is seen to be energy dependent; each sweep takes 2 s for ELS and 4 s for IMS, so it is probable that this is a temporal or spatial variation rather than a true energy dependence since the penetrating background is independent of the analyzer voltage. During the energetic particle shadow, the magnetospheric electrons below ~10 eV show a number of features and time variations: (1) a flux enhancement at ~09:31:26, (2) a dropout at 09:31:30–09:31:34, and (3) a change in the energy of maximum flux between 09:31:36 and 09:31:46.

[18] There is also a separate population at ~15–30 eV (labeled "photoelectrons"). The ions show an overall slowing of the magnetospheric ion population, with the lowest velocity and lowest energy flux seen simultaneously with the electron dropout (feature 2 above).

[19] Feature 1 shows a brief electron flux enhancement and acceleration (probably associated with a spacecraft potential excursion to less negative values, as the magnetic field components show smooth behavior at that time), simultaneous with the beginning of a marked, longer decrease in ion energy associated with flow slowing toward stagnation. It is possible that the electron behavior in feature 3 (see also Figure 4) is also associated with a change in spacecraft potential; this is already negative in this region, and the electron spectra are consistent with slightly less negative values here.

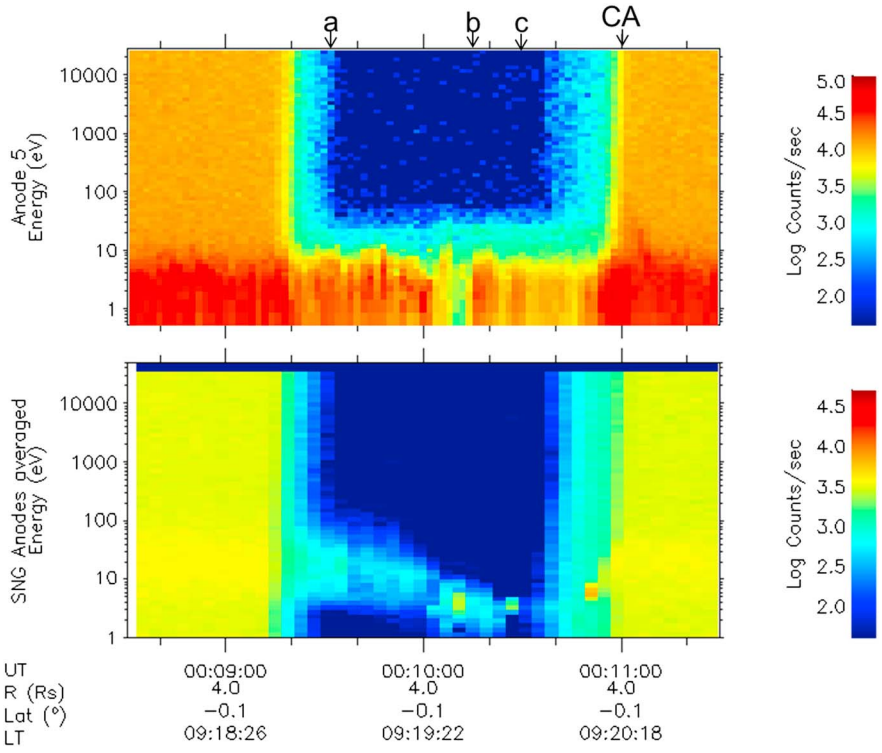

Figure 8. ELS and SNG data from the E9 encounter; format as Figure 4. Times of spectra a, b, and c here refer to Figure 9.

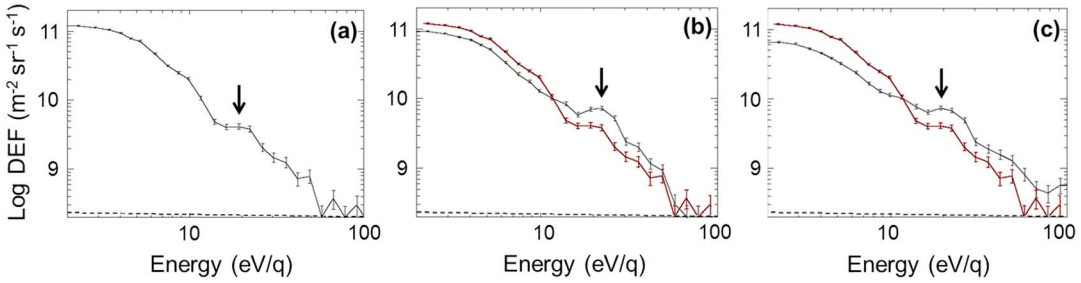

Figure 9. Electron spectra from the E9 encounter, averaged over five sweeps (10 s) from the marked times: (a) 00:09:33, (b) 00:10:15, and (c) 00:10:29.The spectrum in Figure 9a is reproduced in red in Figures 9b and 9c for comparison; format as for Figure 5.

The feature labeled photoelectrons, revealed in detail by the energetic particle shadow, is interpreted as the photoelectrons produced from ionization of neutrals in this region, supplemented by photoelectrons produced within the plume (see below). The time variation evident in the plot is consistent with an enhancement near closest approach, i.e., during plume traversal. The photoelectrons do not follow the behavior exhibited by features 1–3 as they are produced from local ionization of neutrals rather than directly related to Saturn's magnetospheric electrons.

[20] Figure 5 shows a spectrogram over a restricted energy and time range to emphasize feature 4, as well as differential energy flux spectra from (a) before, (b) immediately before, and (c) after feature 2. We should note that the spectrum in Figure 5b includes the short-lived feature 1 and part of feature 2 in the 10 s average. All the spectra clearly show a peak at ~20–22 eV (arrowed) and a sharp reduction in the flux at ~60 eV. The shapes of these features are highly reminiscent of the Saturnian magnetospheric photoelectron signatures modeled and observed by *Schippers et al*. [2009], as well as plume photoelectron spectra modeled by *Ozak et al*. [2012]. We suggest that the spectra in Figures 5a and 5c are magnetospheric photoelectrons, and the spectrum in Figure 5b has an increased flux due to the addition of plume photoelectrons. The energy of the peak (20–22 eV) and the flux reduction at ~60 eV are consistent with the modeled features if we correct the observed data by a spacecraft potential of a few volts negative (J.-E. Wahlund, personal communication, 2012).

[21] In Figure 6, we show 1 min of ELS (top panel) and IMS data (bottom panel) from E19, as well as the variation of electron count rates between 16 and 30 eV (middle panel). The beginning and end of this plot are within the energetic particle shadow; the <10 eV counts show the magnetospheric electrons, and the ~15–50 eV peak is a good indication of the magnetospheric photoelectron flux [cf. *Schippers et al*., 2009]. The top and bottom panels confirm the simultaneous observation of feature 2 in the electrons and the minimum ion energy (related to the ion flow speed), while

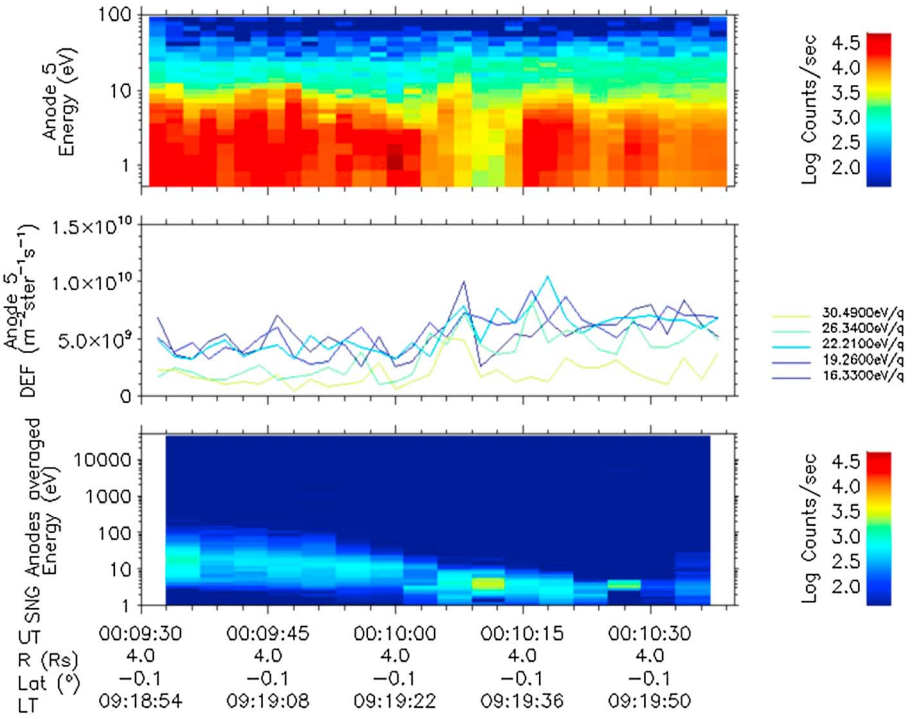

Figure 10. E9 data. (top panel) ELS spectrogram. (middle panel) ELS counts at indicated energies. (bottom panel) IMS spectrogram. Format as for Figure 6.

the line plots in the middle panel show an increase of photoelectron flux within the peak (and over all energies) by a factor ~1.5–2 compared to surrounding values (cf. the spectra in Figures 5a and 5c). We suggest that this increase is associated with photoelectrons from the plume itself, as the peak is still clearly identifiable at this time and is of higher flux than the spectra in Figure 5a or 5c. The energy of the peak is slightly higher in the spectra in Figures 5b and 5c compared to the spectrum in Figure 5a, indicating a slightly less negative spacecraft potential at these times. The later increase in <22 eV flux (between 09:31:40 and 09:31:50) is the result of the increase of the energy of maximum flux in the intense low-energy magnetospheric population observed by ELS (feature 3 above), which as indicated earlier may be due to a change to less negative spacecraft potential.

[22] We examine further the increase of plume photoelectrons within the plume itself by presenting CAPS data from E9. From Table 1, there are a few encounters other than E19 where the ram angle is high, although only E9 provides a suitable fixed-actuator traverse through the plume region. Figure 7 shows the geometry of the E9 encounter, with the closest approach in this case just after Cassini traverses the plume.

[23] Figure 8 shows the ELS and single spectrograms for the E9 encounter. Penetrating radiation is again seen, in this case before ~00:09:30 and after 00:10:40. There is significantly more time variation in the magnetospheric electron flux this time, including a dropout (at ~00:10:07–00:10:13) which is superimposed on a general reduction in the low-energy (<10 eV) electron flux (cf. spectra in Figures 9b and 9c compared to Figure 9a) during the entire energetic particle shadow when the penetrating radiation is absent. The ions show a steady reduction in energy across the energetic particle shadow as Cassini traverses the plume, with a minimum energy at ~00:10:40. The energy reduction occurs contemporaneously with the overall electron flux reduction noted above, and these two features are indicative of the magnetospheric electron behavior. The photoelectrons, on the other hand, are more related to the neutral density and so behave somewhat differently. In addition, any spacecraft potential changes appear less significant in this case than that of E19.

[24] Figure 9 shows electron spectra taken at the intervals indicated on the ELS spectrogram during E9. Both the spectrogram and spectra reveal a peak at ~20 eV. The intensity of this peak increases across the energetic electron shadow. We interpret the spectrum in Figure 9a as the magnetospheric photoelectrons, while the spectra in Figures 9b and 9c represent the sum of magnetospheric and plume photoelectrons, as Cassini moves into the denser, slower ion part of the plume as shown in Figure 8. Again, there is a factor ~2 between the spectra in Figures 9b and 9c, where the plume photoelectrons are observed, and the spectrum in Figure 9a.

[25] Figure 10 shows the electron and ion fluxes for E9 in a similar format to Figure 6. The line plots, together with the spectrogram, further support the observation of an increase in plume photoelectrons toward the right in the plot as Cassini enters the slowest and densest parts of the plume.

[26] From Table 1, E4 is another encounter during which the sampled angular range of anode 5 is well away from the ram direction. Close inspection of the data for this encounter (not shown) also reveals a photoelectron flux which is larger in the plume than away from the plume. This again provides evidence that in the plume the photoelectron spectrum consists of plume and magnetospheric photoelectrons, with only magnetospheric photoelectrons present outside the plume. The ratio of intensities in this case is 2.5.

[27] Reexamination of Figure 1 shows that magnetospheric, and perhaps plume, photoelectrons are present at most or all other encounters, as peaks at ~20 eV are seen in all of the spectrograms where the energetic particle shadow allows a good enough signal-to-noise ratio in the lower energy portion of the electron spectra.

4. Discussion

[28] The variation of the penetrating radiation from encounter to encounter gives an interesting proxy measurement for electrons over 800 keV, in addition to the Magnetosphere Imaging Instrument's low energy magnetospheric measurement system [*Krimigis et al*., 2004] measurements on Cassini. This can clearly provide additional insight into the dynamic properties of the radiation belt population; in particular, we observe a factor of 10 difference between different encounters, showing that Saturn's radiation belts are indeed dynamic. Different spacecraft attitudes may, however, also provide differences to the shielding by the spacecraft during these encounters; detailed study of this is beyond the scope of the current paper.

[29] The removal of the penetrating radiation by the body of Enceladus itself gives an excellent measurement of the other electron (and ion) fluxes near Enceladus throughout the CAPS energy range. The magnetospheric particles show clear evidence of mass loading (ions) and depletion (electrons) presumably to charge dust particles [*Hill et al*., 2012]. The magnetospheric photoelectrons produced throughout the region by the abundance of neutrals in this part of the magnetosphere, some of which undergo ionization, are also clearly apparent [cf. *Schippers et al*., 2009; *Cravens et al*., 2011]. The source of the neutrals is ultimately Enceladus itself, supplemented by the rings.

[30] However, the really new feature seen here is the increase of photoelectron flux in the plume close to Enceladus. This population, together with the magnetospheric photoelectrons, forms a suprathermal population that implies an additional source of ionization (by electron impact, which requires energies > ~13 eV) near to Enceladus, supplementing the ionization produced by magnetospheric photoelectrons. The hot electron component is critical in determining which ionization process dominates: in some calculations [e.g., *Fleshman et al*., 2012], electron impact ionization dominates, whereas in others, photoionization dominates [*Ozak et al*., 2012]. Clearly, additional warm electrons, both the magnetospheric and plume photoelectrons, will increase the importance of collisional ionization.

[31] Ionospheric photoelectrons are present elsewhere in the Saturn system, including at Titan and near the main rings, together with the distributed magnetospheric photoelectron source throughout the inner magnetosphere.

[32] The energy signature of the magnetospheric photoelectrons compares well with that observed by *Schippers et al*. [2009], who also modeled the production of the

photoelectrons from water group-related neutral molecules and radicals. The spectrum of the plume photoelectrons is the same, indicating a similar composition for the parent neutrals. Note that plume photoelectrons have also been modeled in detail by *Ozak et al*. [2012], and our observation supports the photoelectron interpretation at least for the >15 eV electrons.

[33] We note that the plume photoelectrons are seen over a relatively limited region of space, namely within the plume where the neutral density is relatively high, building up to a maximum in the stagnation region. At other objects, including Titan, Mars, and Venus, similar photoelectrons may be transported from their production point (in those cases, the dayside ionospheres). In those cases, the transport is along the magnetic field to remote locations, for example, the tails of these objects [see *Coates et al*., 2011, and references therein], and can be used to indicate a magnetic connection to the production point. This process may also be in operation in the Enceladus plume, although we suggest two reasons which may preclude the unambiguous observation of remote plume photoelectrons. These are as follows:

[34] 1. It would be difficult to distinguish any transported plume photoelectrons, which would have lower flux than those seen in the plume itself, from the separate magnetospheric photoelectron population which pervades Saturn's entire inner magnetosphere region, including the vicinity of Enceladus. As pointed out above, the energy spectrum is the same for the two photoelectron populations, so we cannot uniquely identify the source of the observed fluxes. However, the observed location of higher fluxes of photoelectrons within the plume reveals the source of this population (which we refer to as plume photoelectrons) as ionization of neutrals in the plume.

[35] 2. It is possible that the plume photoelectrons produce impact ionization locally quite rapidly, within the region of higher neutral density, before they can be transported away.

5. Summary and Conclusions

[36] During the energetic particle shadow, when particles from Saturn's radiation belts are shielded by Enceladus itself, a low-energy magnetospheric electron population is observed with a short reduced density interval very near closest approach, possibly associated with flow stagnation [*Tokar et al*., 2009] or with ice grain charging. In addition to this population, an enhanced intensity photoelectron peak is observed consisting of plume photoelectrons added to preexisting magnetospheric photoelectrons. The energy of the enhanced peak is similar to those seen in Saturn's ring environment [*Coates et al*., 2005, and references therein], at Titan [*Coates et al*., 2007, 2011; *Wellbrock et al*., 2012], and in the magnetosphere near Enceladus [*Schippers et al*., 2009] as well as at Mars and Venus [*Coates et al*., 2008, 2011, and references therein]. We interpret the enhanced population as photoelectrons from ionization of the gas and dust species in Enceladus' plume ionosphere.

[37] In summary, the particle populations near Enceladus are complex, including (1) magnetospheric electrons and ions [e.g., *Coates et al*., 2010a, 2010b; *Tokar et al*., 2009], (2) negative [*Coates et al*., 2010a, 2010b] and positive [*Tokar et al*., 2009] water cluster ions [see also *Coates*, 2012], (3) charged nanograins [*Jones et al*., 2009; *Hill et al*., 2012], (4) magnetospheric photoelectrons [*Schippers et al*., 2009; *Cravens et al*., 2011, this paper], and (5) plume photoelectrons (this paper) providing a factor 1.5–2.5 increase in the electron flux at ~20 eV.

[38] The shielding by Enceladus itself reveals the latter two populations of photoelectrons which are from Saturn's neutral cloud and from the Enceladus plume, respectively.

[39] The plume photoelectrons are clearly seen during E19, E9, and E4 (not shown), where the CAPS field of view precluded observations of the ram species (water clusters and charged dust). We also observe the presence of magnetospheric and plume photoelectrons at most/all other Enceladus encounters. The results indicate that an additional ionization source (the relatively warm photoelectrons) should be included in models, increasing the importance of electron impact ionization.

[40] **Acknowledgments.** We thank L.K. Gilbert and G.R. Lewis for software support. We acknowledge support of CAPS ELS science by STFC and of the CAPS ELS operations and software team by ESA via the UK Space Agency (from 2011). C.S.A. was supported by a Royal Society research fellowship. Work in the U.S. was supported by NASA JPL contracts 1243218 and 1405851 to the Southwest Research Institute. Work at Los Alamos was conducted under the auspices of the U. S. Department of Energy, with support from NASA's Cassini project.

[41] Masaki Fujimoto thanks Elias Roussos and another reviewer for their assistance in evaluating this paper.

References

Brace, L. H., R. F. Theis, and W. R. Hoegy (1982), Plasma clouds above the ionopause of Venus and their implications, *Planet. Space Sci.*, *30*, 29–37.

Coates, A. J. (2012), Enceladus, in *McGraw-Hill Yearbook of Science & Technology 2012*, pp. 72–76, McGraw-Hill, New York.

Coates, A. J., A. D. Johnstone, J. F. E. Johnson, J. J. Sojka, and G. L. Wrenn (1985), Ionospheric photoelectrons observed in the magnetosphere at distances of up to 7 earth radii, *Planet. Space Sci.*, *33*, 1267–1275.

Coates, A. J., et al. (2005), Plasma electrons above Saturn's main rings: CAPS observations, *Geophys. Res. Lett.*, *32*, L14S09, doi:10.1029/2005GL022694.

Coates, A. J., F. J. Crary, D. T. Young, K. Szego, C. S. Arridge, Z. Bebesi, E. C. Sittler Jr., R. E. Hartle, and T. W. Hill (2007), Ionospheric electrons in Titan's tail: Plasma structure during the Cassini T9 encounter, *Geophys. Res. Lett.*, *34*, L24S05, doi:10.1029/2007GL030919.

Coates, A. J., et al. (2008), Ionospheric photoelectrons at Venus: Initial observations by ASPERA-4 ELS, *Planet. Space Sci.*, *56*, 802–806.

Coates, A. J., G. H. Jones, G. R. Lewis, A. Wellbrock, D. T. Young, F. J. Crary, R. E. Johnson, T. A. Cassidy, and T. W. Hill (2010a), Negative ions in the Enceladus plume, *Icarus*, *206*, 618–622.

Coates, A. J., A. Wellbrock, G. R. Lewis, G. H. Jones, D. T. Young, F. J. Crary, J. H. Waite, R. E. Johnson, T. W. Hill, and E. C. Sittler Jr. (2010b), Negative ions at Titan and Enceladus: Recent results, *Faraday Disc.*, *147*(1), 293–305, doi:10.1039/C004700G2010.

Coates, A. J., S. M. E. Tsang, A. Wellbrock, R. A. Frahm, J. D. Winningham, S. Barabash, R. Lundin, D. T. Young, and F. J. Crary (2011), Ionospheric photoelectrons: Comparing Venus, Earth, Mars and Titan, *Planet. Space Sci.*, *59*, 1019–1027.

Coates, A. J., et al. (2012), Cassini in Titan's tail: CAPS observations of plasma escape, *J. Geophys. Res.*, *117*, A05324, doi:10.1029/2012JA017595.

Cravens, T. E., N. Ozak, M. S. Richard, M. E. Campbell, I. P. Robertson, M. Perry, and A. M. Rymer (2011), Electron energetics in the Enceladus torus, *J. Geophys. Res.*, *116*, A09205, doi:10.1029/2011JA016498.

Dougherty, M. K., K. K. Khurana, F. M. Neubauer, C. T. Russell, J. Saur, J. S. Leisner, and M. E. Burton (2006), Identification of a dynamic atmosphere at Enceladus with the Cassini magnetometer, *Science*, *311*, 1406–1409.

Esposito, L. W., et al. (2005), Ultraviolet imaging spectroscopy shows an active Saturnian system, *Science*, *307*, 1251–1255.

Farrell, W. M., W. S. Kurth, D. A. Gurnett, R. E. Johnson, M. L. Kaiser, J.-E. Wahlund, and J. H. Waite Jr. (2009), Electron density dropout near Enceladus in the context of water-vapor and water-ice, *Geophys. Res. Lett.*, *36*, L1020, doi:10.1029/2008GL037108.

Fleshman, B. L., P. A. Delamere, F. Bagenal, and T. Cassidy (2012), The roles of charge exchange and dissociation in spreading Saturn's neutral clouds, *J. Geophys. Res.*, *117*, E05007, doi:10.1029/2011JE003996.

Frahm, R. A., et al. (2006), Carbon dioxide photoelectron peaks at Mars, *Icarus*, *182*, 371–382.

Hill, T. W., et al. (2012) Charged nanograins in the Enceladus plume, *J. Geophys. Res.*, *117*, A05209, doi:10.1029/2011JA017218.

Jones, G. H., E. Roussos, N. Krupp, C. Paranicas, J. Woch, A. Lagg, D. G. Mitchell, S. M. Krimigis, and M. K. Dougherty (2006), Enceladus' varying imprint on the magnetosphere of Saturn, *Science*, *311*, 1412–1415.

Jones, G. H., et al. (2009), Fine jet structure of electrically charged grains in Enceladus' plume, *Geophys. Res. Lett.*, *36*, L16204, doi:10.1029/2009GL03828.

Kollmann, P., E. Roussos, C. Paranicas, N. Krupp, C. M. Jackman, E. Kirsch, and K.-H. Glassmeier (2011), Energetic particle phase space densities at Saturn: Cassini observations and interpretations, *J. Geophys. Res.*, *116*, A05222, doi:10.1029/2010JA016221.

Krimigis, S. M., et al. (2004), Magnetosphere Imaging Instrument (MIMI) on the Cassini Mission to Saturn/Titan, *Space Sci. Rev.*, *114*, 233–329.

Linder, D. R., A. J. Coates, R. D. Woodliffe, C. Alsop, A. D. Johnstone, M. Grande, A. Preece, B. Narheim, K. Svenes, and D. T. Young (1998), The Cassini CAPS electron spectrometer, in *Measurement Techniques in Space Plasmas: Particles*, *Geophys. Monogr. Ser.*, vol. 102, edited by R. E. Pfaff, J. E. Borovsky, and D. T. Young, pp. 257–262, AGU, Washington, D. C.

Ozak, N., T. E. Cravens, G. H. Jones, A. J. Coates, and I. P. Robertson (2012), Modeling of electron fluxes in the Enceladus plume, *J. Geophys. Res.*, *117*, A0622, doi:10.1029/2011JA017497.

Perry, M. E., B. Teolis, H. T. Smith, R. L. McNutt, G. Fletcher, W. Kasprzak, B. Magee, D. G. Mitchell, and J. H. Waite Jr. (2010), Cassini INMS observations of neutral molecules in Saturn's E-ring, *J. Geophys. Res.*, *115*, A10206, doi:10.1029/2010JA015248.

Porco, C. C., et al. (2006), Cassini observes the active south pole of Enceladus, *Science*, *311*, 1393–1401.

Pryor, W. R., et al. (2011), The auroral footprint of Enceladus on Saturn, *Nature*, *472*, 331–333.

Roussos, E., G. H. Jones, N. Krupp, C. Paranicas, D. G. Mitchell, A. Lagg, J. Woch, U. Motschmann, S. M. Krimigis, and M. K. Dougherty (2007), Electron microdiffusion in the Saturnian radiation belts: Cassini MIMI/LEMMS observations of energetic electron absorption by the icy moons, *J. Geophys. Res.*, *112*, A06214, doi:10.1029/2006JA012027.

Rymer, A. M., A. J. Coates, G. A. Abel, D. R. Linder, K. Svenes, B. Narheim, M. Thomsen, and D. T. Young (2001), Cassini CAPS electron spectrometer measurements during the Earth swing-by on 18 August 1999, *J. Geophys. Res.*, *106*, 30,177–30,198.

Rymer, A. M., et al. (2007), Electron sources in Saturn's magnetosphere, *J. Geophys. Res.*, *112*, A02201, doi:10.1029/2006JA012017.

Schippers, P., N. Andre, R. E. Johnson, M. Blanc, I. Dandouras, A. J. Coates, S. M. Krimigis, and D. T. Young (2009), Identification of photoelectron energy peaks in Saturn's inner neutral torus, *J. Geophys. Res.*, *114*, A12212, doi:10.1029/2009JA014368.

Schunk, R. W., and A. F. Nagy (2009), *Ionospheres: Physics, Plasma Physics, and Chemistry*, Cambridge University Press, Cambridge, U. K.

Shemansky, D. E., P. Matheson, D. T. Hall, H.-Y. Hu, and T. M. Tripp (1993), Detection of the hydroxyl radical in the Saturn magnetosphere, *Nature*, *363*, 329–331.

Spahn, F., et al. (2006), Cassini dust measurements at Enceladus and implications for the origin of the E ring, *Science*, *311*, 1416–1418.

Tokar, R. L., et al. (2006), The Interaction of the atmosphere of Enceladus with Saturn's plasma, *Science*, *311*, 1409–1412.

Tokar, R. L., R. E. Johnson, M. F. Thomsen, R. J. Wilson, D. T. Young, F. J. Crary, A. J. Coates, G. H. Jones, and C. S. Paty (2009), Cassini detection of Enceladus' cold water-group plume ionosphere, *Geophys. Res. Lett.*, *36*, L13203, doi:10.1029/2009GL038923.

Waite, J. H., et al. (2006), Cassini ion and neutral mass spectrometer: Enceladus plume composition and structure, *Science*, *311*, 1419–1422.

Wellbrock, A., A. J. Coates, I. Sillanpää, G. H. Jones, C. S. Arridge, G. R. Lewis, D. T. Young, F. J. Crary, and A. D. Aylward (2012), Cassini observations of ionospheric photoelectrons at large distances from Titan: Implications for Titan's exospheric environment and magnetic tail, *J. Geophys. Res.*, *117*, A03216, doi:10.1029/2011JA017113.

Young, D. T., et al. (2004), Cassini plasma spectrometer investigation, *Space Sci. Rev.*, *114*, 1–112.

Young, D. T., et al. (2005), Composition and dynamics of plasma in Saturn's magnetosphere, *Science*, *307*, 1262–1265.